Research article

Thermally reduced graphene/polyethylene nanocomposites: effects of graphene on isothermal and nonisothermal crystallization of polyethylene

Ahmed Z.A. Abuibaid, Muhammad Z. Iqbal *

Department of Chemical and Petroleum Engineering, United Arab Emirates University, PO Box 15551, Al-Ain, United Arab Emirates

ARTICLE INFO

ABSTRACT

The crystallization behavior of polyethylene/thermally reduced graphene (PE/TRG) nanocomposites prepared via solvent blending is investigated using a differential scanning calorimeter, and results are compared with PE/carbon black (CB) composites. The effects of TRG and CB concentrations on the crystallization process are studied under isothermal and dynamic conditions. The Avrami and modified Avrami equations provided excellent fits to isothermal and dynamic crystallization kinetics data, respectively. The TRG nanosheets acted as nucleating agents during crystallization attributed to substantial decrease in crystallization half time at higher TRG concentrations. The reduced surface energy of the nanocomposites with incorporation of TRG further confirmed its nucleating behavior.

1. Introduction

Semicrystalline polymers such as polyolefins constitute an important class of polymers for nanocomposite applications. The glassy (amorphous) to rubbery transition in semicrystalline polymers is defined by glass transition (T_g), whereas polymers turn from solid to liquid state (phase change) at their melting point (T_m). Polymers crystallize when cooled from melt or heated from an amorphous state to temperatures between T_g and T_m. Due to significant amorphous fractions in semicrystalline polymers, the crystallization process can result in various forms of crystal structures. The overall kinetics of crystallization are governed by a degree of conversion and conversion rate, irrespective of the structures encountered. Practically, physical properties of polymers strongly depend on structures formed during processing operations [1]. Polymers can crystallize isothermally (at selected temperatures) or nonisothermally (under dynamic conditions). The isothermal crystallization is mostly used for theoretical analysis. However, various processing methods such as extrusion are performed under dynamic conditions. Therefore, quantifying and parametrization of the crystallization rates is pertinent in optimizing industrial processes.

Generally, the surface area-to-volume ratio increases with decreasing filler particle size. A hundred-fold increase in surface area, results from a ten-fold decrease in particle diameter (main attraction towards nanofillers). In nanocomposites, an interfacial polymer layer (shell) attaches with large surface area filler (core), forming an interface. Typically,

nanocomposites filled with less than 5 vol.% filler are considered interfacial composites [1] where a large proportion of molecular chains is located at the interface. The chain mobility is hindered in the shell compared to that in bulk material, resulting in chain confinement effects leading to increased glass transition. On the other hand, reverse is true for noninteracting polymer/filler interfacial forces. The interfacial adhesion is a function of polymer structure at the interface (shell), resulting in varied crystallinity and morphology [1, 2] of nanocomposites. The mechanical properties of nanocomposites are also a strong function of the interfacial adhesion. Therefore, understanding crystallization behavior of the shell is of great practical importance for understanding product formation processes.

Among various methods of synthesizing graphene, thermal exfoliation of graphite oxide resulting in thermally reduced graphene (TRG) is a top-down method for bulk production of graphene [3]. TRG exhibits contains few layers of 200 nm to a few microns wide graphene sheets with a thickness of 1–5 nm per TRG particle [4]. Typically, exceptionally high properties of graphene makes it a versatile filler for polymer nanocomposites applications [5]. In graphene/polyethylene (PE) nanocomposites, Cheng et al. [6] reported crystallization of PE/reduced graphene oxide and showed accelerated crystallization of PE nanocomposites with improved thermal stability compared to neat PE. A similar conclusion was reached by Fan et al. [7] using compatibilized nanoclay/PE nanocomposites where nanoclay acted as a heterogeneous nucleating agent promoting the crystallization. Tarani et al. [8] reported
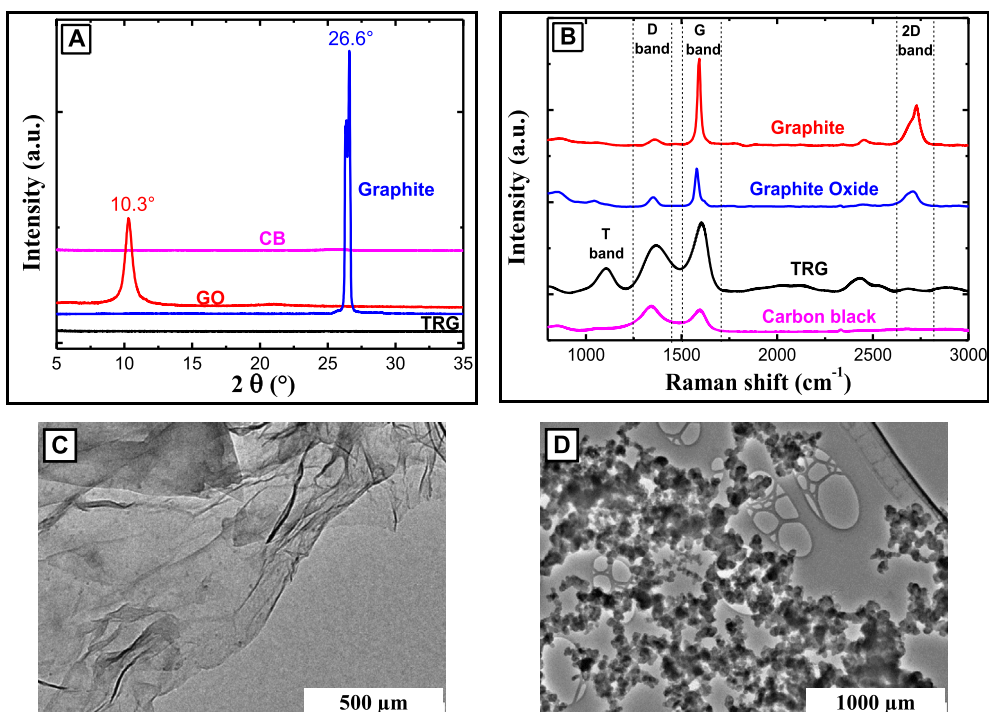

Figure 1. X-ray diffraction traces (A) and Raman spectra of graphite, GO, TRG, and CB (B). TEM images of graphene (C) and CB (D).

fast crystallization of graphene/high density polyethylene (HDPE) nanocomposites with variable graphene particle diameters. Higher cooling rates during nonisothermal crystallization formed small-scale ordered-domains, lacking high-ordered structures in HDPE. In addition, bigger particles produced crystals with increased aggregate size. Recently, Iqbal et al. [9] reported PE/TRG nanocomposites and showed marked improvement in mechanical and electrical properties of the

nanocomposites via blending PE with oxidized PE. The increased properties were attributed to microstructural changes induced by TRG and oxidized PE into the PE structure. However, no crystallization data was reported to elaborate the structural changes in PE. This paper is a continuation of the above work focusing the effects of TRG on crystallization of PE/TRG nanocomposites. The kinetics of isothermal and nonisothermal crystallization are investigated at varying graphene loadings.
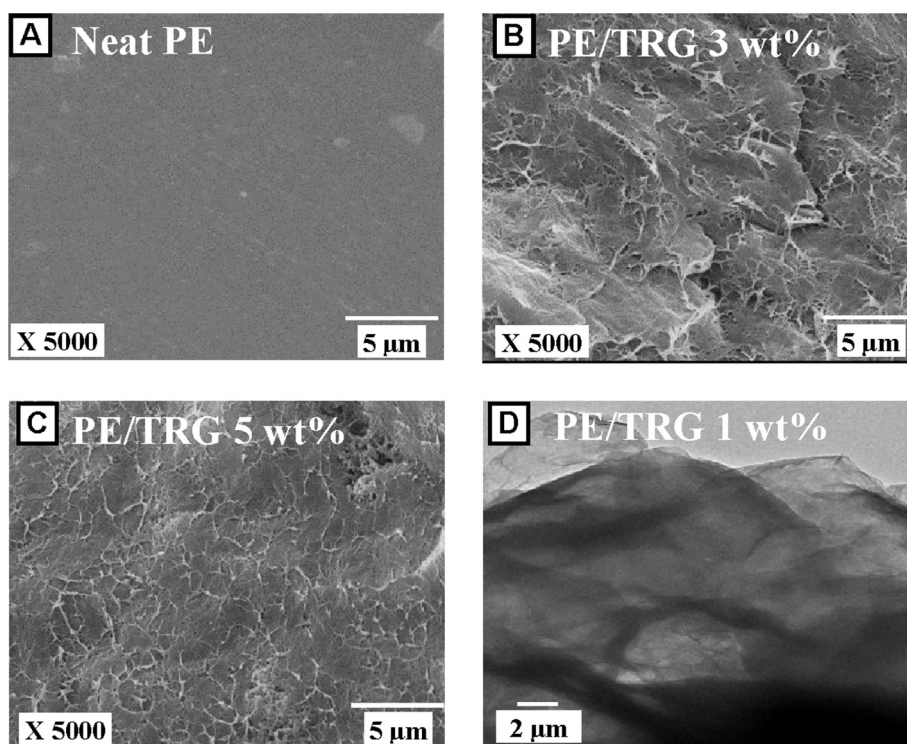

Figure 2. SEM of neat PE (A), PE/TRG 3 wt% (B), PE/TRG 5 wt% (C), and TEM image of PE/TRG 1 wt% (D).
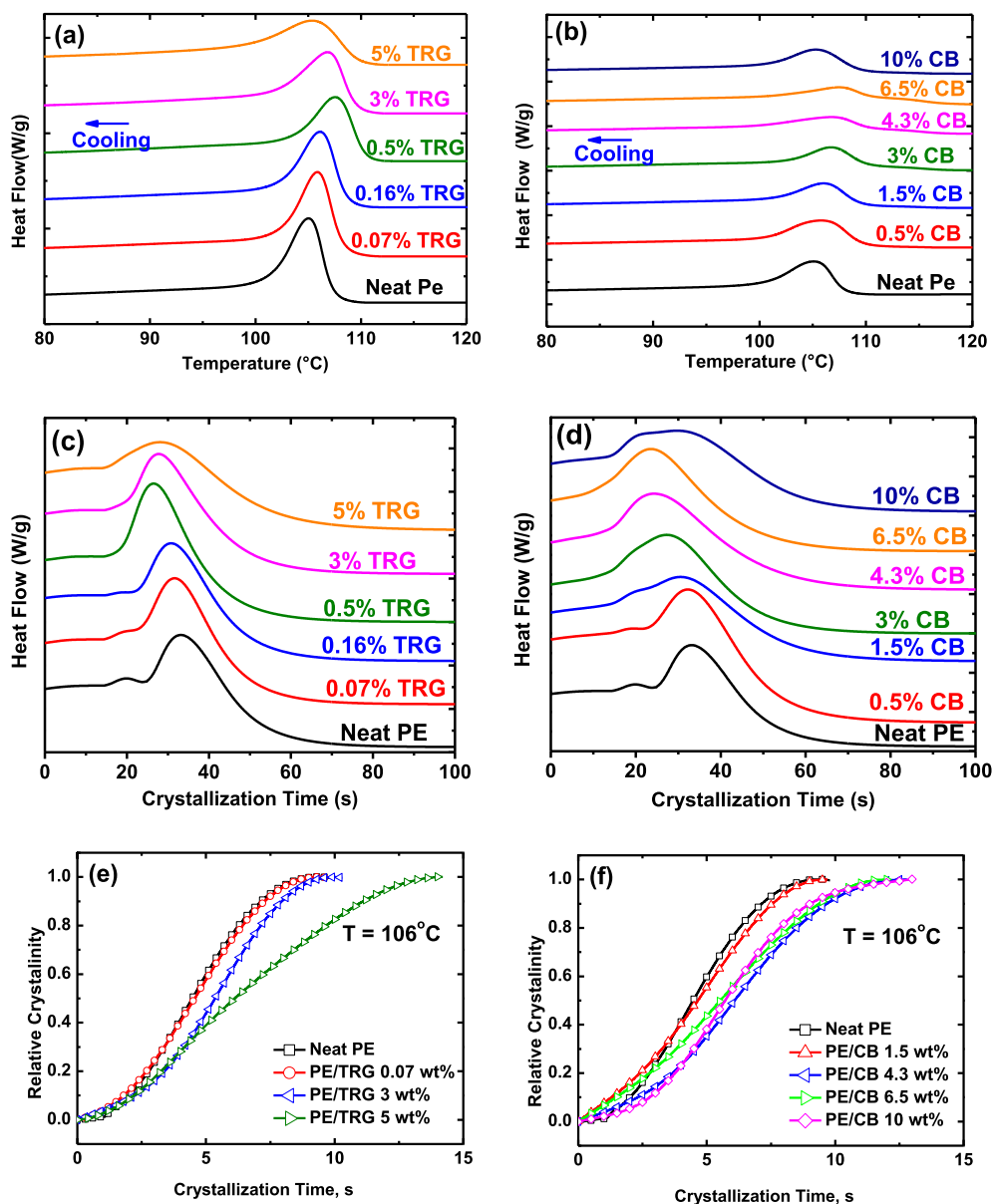
Figure 3. Cooling profiles of a) PE/TRG nanocomposites and b) PE/CB composites (cooling = 10 °C/min). Isothermal crystallization of c) PE/TRG and d) PE/CB (at 106 °C), and relative crystallinity of PE/TRG (e) and PE/CB composites (f). (Marker points in (e) and (f) show experimental data and solid lines indicate the Avrami fit).

The results are also compared with conventional carbon black filled PE composites used commercially. The PE/CB crystallization data is provided in the supplementary information, and only pertinent results are reported in the main document here.

2. Experimental details

2.1. Materials

Linear low-density polyethylene (LLDPE) with a bulk density 0.97 g/cm^3 (428078, lot#07730MEV, Sigma Aldrich), carbon black (CB) (99.9%, bulk density = 170–230 g/L, surface area = 75 m^2/g, Alfa Aesar), or Natural flake graphite (-10 mesh, 99.9% Alfa Aesar). p-xylene (99%, Sigma Aldrich), potassium permanganate (Fisher Scientific), sulfuric acid (95–97%, J.T. Bakers), phosphoric acid (>99%, Aldrich), hydrogen peroxide (30% solution, BDH), HCl (37%, Reidel-deHaen), were used as received.

2.2. Synthesis of thermally reduced graphene (TRG)

TRG was synthesized using a two-step approach: 1) oxidation of graphite, and 2) thermal exfoliation of graphite oxide into TRG. GO was synthesized following Tour's method [10, 11]. TRG was produced thermally exfoliating GO [3, 9, 10]. Briefly, graphite (~5 g) was dispersed in a ~8.2/1 vol/vol mixture of H$_2$SO$_4$/H$_3$PO$_4$ for 30 min at room temperature via magnetic stirring. Approximately 28g of KMNO$_4$ was added into graphite dispersion (3–5 min) and stirred for 72 h using an overhead stirrer at room temperature. Upon completion of the reaction, a mixture of 30% H$_2$O$_2$ and deionized water (17.5/137.5 mL/mL) was added to the dispersion after 72 h while stirring until dark brown color transformed to bright yellow, indicating formation of GO. GO was washed 3 times with 1 M HCl aqueous solution and multiple times with deionized water until a pH of 4–5 was obtained, indicating removal of unreacted impurities. GO solution was centrifuged at 10,000 g force followed by dialysis. GO was further dried in a vacuum drying over 48 h to remove adsorbed water.

Table 1. Thermal characteristics of PE/TRG nanocomposites.

PE/TRG (wt %)	1st Cooling Scan				2nd Heating Scan		
	Onset T_c (°c)	Peak end T_c (°c)	Peak T_c (°c)	ΔH_c (J/g)	Peak T_m (°c)	ΔH_m (J/g)	X_c (%)
0	107.4	34.8	105.0	101.11	122.0	93.52	33.52
0.07	108.3	32.7	104.8	104.83	121.5	94.01	33.72
0.16	108.7	34.8	106.1	100.01	121.9	91.79	32.95
0.5	110.4	31.2	107.5	103.88	122.1	95.53	34.41
3	109.6	32.9	106.8	100.4	121.8	94.26	34.83
5	109.8	34.2	105.4	94.741	122.4	85.92	32.42

Table 2. Thermal characteristics of PE/CB composites.

PE/CB (wt%)	1st Cooling Scan				2nd Heating Scan		
	Onset T_c (°c)	Peak end T_c (°c)	Peak T_c (°c)	ΔH_c (J/g)	Peak end T_c (°c)	ΔH_m (J/g)	X_c (%)
0	107.4	34.8	105.0	101.11	122.0	93.52	33.52
0.5	109.8	37.6	105.8	103.46	121.7	101.31	36.34
1.5	109.8	34.2	106.0	96.62	122.7	92.47	33.20
3	110.7	33.0	106.7	96.89	122.6	89.82	32.35
4.3	111.5	35.9	106.7	92.02	123.1	86.59	31.99

Table 3. Summary of isothermal analysis of PE/TRG nanocomposites.

TRG wt%	From thermal data					Avrami Theory				LH-Theory	
	T_c (°C)	T_m (°C)	T^o_m (°C) £	ΔH_m (J/g)	X_c %	$t_{1/2}$*	$t_{1/2}$**	K (×10²)	n	K_g (K²)	σ_e (kJ/m²)
0	106	122.2	124.0	96.1	34.5	4.4	4.5	1.68	2.5	12640	6.03
	108	122.4		95.8	34.3	5.2	5.3	1.32	2.4		
	110	122.6		95.0	34.1	8.2	8.2	1.14	1.95		
	112	122.2		96.8	34.7	9.5	9.4	1.54	1.69		
0.07	106	121.5	121.8	96.0	34.4	4.5	4.6	1.97	2.37	14178	6.81
	108	121.3		95.2	34.2	5.2	5.3	1.52	2.31		
	110	121.6		95.1	34.1	8.6	8.7	0.65	2.17		
	112	123.9		95.1	34.1	15.5	15.8	0.21	2.11		
0.16	106	121.9	121.9	91.0	32.7	3.7	3.8	4.50	2.09	12063	5.79
	108	121.8		90.1	32.4	4.9	5	1.77	2.31		
	110	121.9		90.0	32.3	6	6.2	2.80	1.79		
	112	123.3		89.0	31.9	11.1	11.4	0.86	1.82		
0.5	106	122.1	121.2	94.3	34.0	7.8	7.9	0.03	3.75	5751	2.77
	108	121.6		93.7	33.7	4.8	4.8	1.05	2.67		
	110	121.9		92.9	33.5	4.2	4.3	3.05	2.17		
	112	123.0		97.4	35.1	7	7.1	1.22	2.07		
3	106	121.9	121.0	94.3	34.9	5.2	5.4	0.74	2.74	5992	2.88
	108	121.5		93.1	34.4	3.9	3.9	3.08	2.3		
	110	121.7		92.9	34.3	4.4	4.5	3.36	2.03		
	112	123.4		92.5	34.2	8.7	8.9	1.21	1.87		
5	106	122.6	122.5	85.6	32.3	6.1	6.1	2.19	1.91	3076	1.47
	108	122.4		84.5	31.9	3.5	3.6	2.60	2.6		
	110	122.6		84.1	31.7	5.2	5.3	4.11	1.71		
	112	122.9		87.5	33.0	6.2	6.3	2.81	1.75		

£ Calculated from Hoffman-Weeks plots using ref [28].
$t_{1/2}$* calculated using equation [3].
$t_{1/2}$** obtained from Figure 3 e and f.

The dried GO was rapidly heated at 1000 °C for 30 s in a tube furnace under inert gas flow to produce thermally reduced graphene (TRG). Furthermore, TRG was dried for 8 h under vacuum.

2.3. Synthesis of nanocomposites via solvent blending

Linear low-density polyethylene (PE) was dissolved in p-xylene at 120 °C for one hour. Meanwhile, graphene was sonicated in p-xylene for one

Table 4. Parameters summary for PE/CB composites with increasing CB wt%.

CB wt%	From thermal data					Avrami Theory				LH- Theory	
	T_c (°C)	T_m	T^o_m (°C) [£]	ΔH_m (J/g)	X_c %	$t_{1/2}$* (s)	$t_{1/2}$** (s)	K ($\times 10^2$)	n	K_g	σ_e ($\times 10^3$)
0	106	122.2	124.1	96.1	34.5	4.4	4.5	1.68	2.5	12565	6.00
	108	122.4		95.8	34.3	5.2	5.3	1.32	2.4		
	110	122.7		95.0	34.1	8.2	8.2	1.14	2.0		
	112	122.2		94.5	33.9	9.5	9.4	1.54	1.7		
0.5	106	121.9	123.7	101.1	36.4	5.2	5.2	1.17	2.5	15641	7.47
	108	122.0		101.8	36.7	5.2	5.3	1.76	2.2		
	110	122.4		100.7	36.3	8.3	8.4	0.75	2.1		
	112	122.7		101.0	36.4	13.7	13.9	0.33	2.1		
1.5	106	122.4	124.6	93.6	34.0	4.5	4.7	2.92	2.1	14971	7.14
	108	122.6		92.7	33.7	3.0	3.0	6.84	2.1		
	110	122.9		91.7	33.4	5.6	5.7	1.62	2.2		
	112	122.7		97.9	35.6	9.4	9.4	0.72	2.0		
3	106	122.3	124.4	90.4	33.4	3.3	3.5	13.20	1.4	8152	3.89
	108	122.5		89.1	31.9	5.4	5.5	0.68	2.8		
	110	122.7		88.2	31.6	6.3	6.4	0.15	3.4		
	112	122.4		96.3	34.5	5.8	5.9	0.27	3.2		
4.3	106	122.9	123.3	88.9	33.3	6.0	6.1	0.93	2.4	-6408	-3.07
	108	122.9		86.6	32.4	4.7	4.6	1.73	2.4		
	110	123.0		85.7	32.1	3.1	3.1	7.56	2.0		
	112	123.5		90.4	33.9	3.5	3.6	4.72	2.1		
6.5	106	121.9	123.3	87.4	33.5	5.3	5.5	2.47	2.0	-5558	-2.66
	108	122.0		86.9	33.3	3.8	4.0	4.55	2.0		
	110	122.2		86.5	33.2	2.8	2.8	10.64	1.8		
	112	122.1		91.6	35.1	3.3	3.4	5.91	2.1		
10	106	123.0	124.8	89.1	35.5	5.7	5.7	0.70	2.6	-9299	-4.43
	108	123.2		87.7	34.9	4.4	4.4	1.32	2.7		
	110	123.4		86.0	34.2	2.6	2.7	10.92	1.9		
	112	123.0		94.0	37.4	3.1	3.2	6.22	2.1		

[£] Calculated from Hoffman-Weeks plots using ref [28].

$t_{1/2}$* calculated using equation [4].

$t_{1/2}$** obtained from Figure 3 e and f.

hour at room temperature. Graphene dispersion was added into PE solution followed by continues stirring for one hour at 120 °C under reflux. The composite solution was drop casted on a heated glass plate at 80 °C and allowed to evaporate the solvent. A complete description of the nanocomposite synthesis methodology is reported in our previous work [9].

2.4. Melt crystallization using differential scanning calorimetry

Melt crystallization of nanocomposites was studied using a modulated differential scanning calorimeter (Discovery DSC 25, TA Instruments). The standard melting and crystallization temperatures were recorded using the following procedure: approximately 5–10 mg sample was heated from 20 °C to 140 °C (above T_m) at 20 °C/min to eliminate previous history followed by cooling to 20 °C at 10 °C/min to record crystallization temperature (T_c). Subsequently heating the sample to 140 °C at same rate was performed to record T_m.

For isothermal kinetics, samples were cooled to selected T_c at 60 °C/min to prevent premature crystallization after the second heat and kept isothermally at T_c for 10 min. This time was optimized after various trials form complete crystallization of all samples. After crystallization was achieved, samples were cooled to 20 °C (equilibrium temperature) followed by heating up to 140 °C at 10 °C/m to record T_m of the crystals. Similar procedure was followed for variously selected crystallization

temperatures. For non-isothermal kinetics, history-removed samples were cooled from T_m in the 2nd cycle to 20 °C at varying cooling rates (2, 5, 10, 15 and 20 °C/min), and development of crystallization peak was recorded. The DSC experiments were conducted under inert atmosphere (N_2 at 50 mL/min).

2.5. Characterization tools

An X'Pert3 Powder X-ray Diffractometer (XRD) from Malvern Panalytical was used for structural analysis. The XRD scans (within 2Θ range of 5–35°) were carried out at a scan speed of 0.02°/s with instrument parameters of 40 kV voltage, 20 A intensity and 1.5406 Å CuKα radiation. Morphology of fractured polymer nanocomposites (gold sputter coated for 3 min) was studied using a JCM-5000 NeoScope scanning electron microscope (SEM) at 15 kV. The morphology of TRG and its dispersion in polymer nanocomposite samples was studied using transmission electron microscope (TEM) (FEI Phillips C200 at 200 kV). For sheet morphology, a small amount of TRG was dispersed in acetone (0.1 mg/mL acetone) via sonication for 10 min and one drop of dispersion was deposited on a 300-mesh Cu grid with holy carbon. For nanocomposites, samples were cut in thin slices using a diamond knife [9]. The Raman spectra were obtained using XploRA ONE confocal Raman spectrometer from Horiba Scientific. Each run war carried out at 532 nm as excitation source and under grafting speed 1800 g/mm (focus: 10×).
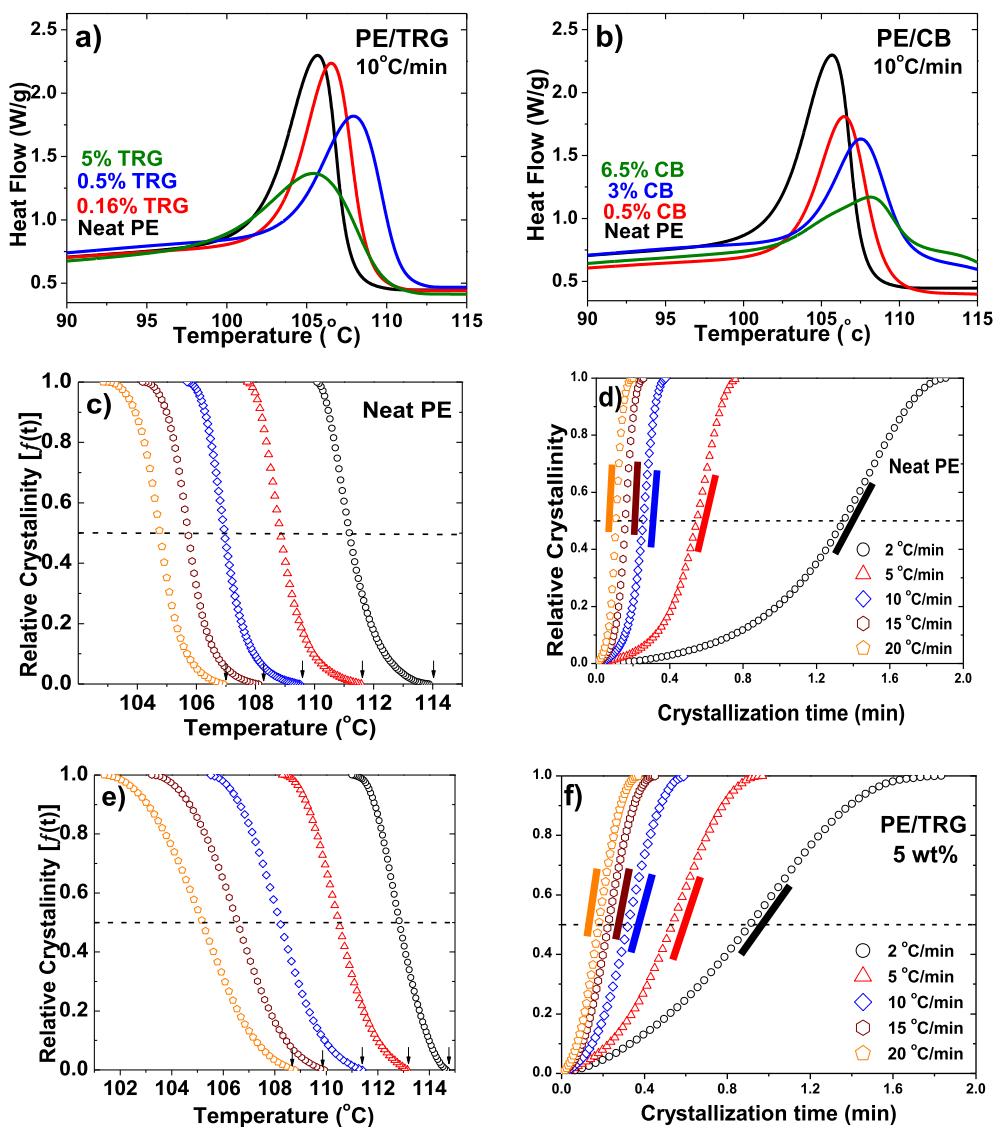
Figure 4. Nonisothermal crystallization thermograms of selected samples a) PE/TRG, b) PE/CB (Cooling rate = 10 °C/min). Relative crystallinity versus c) temperature and d) crystallization time. (The dotted line indicates 50% of crystallization during the evolution of crystallinity).(The arrow signs in right panels indicate the onset of crystallization temperatures). [Marker points represent experimental data and smooth lines the Avrami fit].

3. Results and discussion

3.1. Characterization of TRG and CB

The synthesis of TRG was confirmed using XRD (Figure 1A). A perfectly packed and layered structure of graphite with intrinsic [002] peak at $2\theta = 26.59°$ was observed, showing an interlayer *d*-spacing of ~3.44 Å (using the Bragg's law) and average particle size of 519 Å (Scherrer equation [12]). The [002] peak shifted to lower diffraction angle of $2\theta = 10.3°$ with oxidation in GO (*d*-spacing ~ 8.6 Å and particle size ~104 Å). A low intensity wider [002] peak in GO is attributed to a loosely packed expanded structure where the interlayer spacing is almost doubled. No noticeable diffraction peak was observed in TRG showing a complete exfoliation of GO into graphene nanosheets. On the other hand, CB comprises of spherically shaped carbon particles without any regular pattern (no XRD peak). The CB particles agglomerate in the form of fractals [13] (discussed later in TEM image).

The Raman spectra of graphite, CB, GO, and TRG are shown in Figure 1B. Raman spectroscopy provides useful information about the 1) structural defects (D-band), 2) in-plane saturated C-structure (G-band), and 3) the height of the stack (2D or G′-band) in graphitic structures [14].

The D-band was observed between 1313-1400 cm^{-1} and G-band appeared between 1550-1630 cm^{-1}. The 2D band, caused by splitting photons with opposite momentum, appeared between 2500-2800 cm^{-1} [15]. The intensity and shape of 2D band determines the number of layers in graphitic particles. A very small D-band peak and a sharp G-band peak in graphite indicated a perfectly stacked defect-free structure. The oxidation resulted in introducing defects in graphite indicated by increased D-band intensity. However, a reduction in G-band intensity in GO is attributed to expanded structure in GO. TRG exhibited a large change in D- and G-bands. The D-band increased significantly, and G-band reduced to a value closer to that of D-band. The increased defects in TRG are attributed to thermal treatment. There was no prominent 2D band in TRG, indicating that TRG is mostly composed of single layer graphene sheets. In addition, T-peak appears due to the sp^3 vibration of single bonds between carbons atoms within the Raman UV excitation range (~1108 cm^{-1}) [16]. The D- and G-bands in CB appeared at the same positions as in TRG. Both materials (CB and TRG) did not show 2D band, indicating absence of the layered structure.

A paper-like morphology of graphene sheets was observed in TEM (Figure 1C). The TEM image showed thin, wrinkled, and transparent sheets of graphene where dark fields observed over the dark edges are

Table 5. Nonisothermal crystallization parameters for PE/TRG.

TRG wt%	ϕ	T_o	T_p	$t_{1/2}$	ΔH_c	Avrami Fitting		
	(°C/min)	(°C)	(°C)	(s)	(J/g)	n	k_c (min) (10)	R^2
0	2	112.7	110.0	80.9	114.2	2.0	4.1	0.998
	5	111.0	107.8	32.8	106.0	1.2	7.5	0.996
	10	108.3	105.7	15.3	104.8	1.5	10.2	0.993
	15	106.8	104.2	9.5	103.2	1.8	11.3	0.993
	20	105.9	103.0	6.4	101.0	1.7	11.2	0.994
0.07	2	113.5	110.5	95.8	112.7	1.4	2.2	0.996
	5	112.0	108.3	36.6	115.4	1.2	7.5	0.998
	10	110.0	106.3	19.4	111.6	1.3	9.5	0.997
	15	108.5	104.8	12.8	106.6	1.5	10.4	0.994
	20	108.0	103.6	9.4	106.7	1.4	10.4	0.997
0.16	2	114.1	110.9	77.8	119.0	2.1	4.6	0.996
	5	112.1	108.7	32.7	109.4	1.2	7.7	0.999
	10	110.3	106.6	17.2	105.9	1.4	9.9	0.995
	15	108.5	105.1	11.3	104.3	1.7	10.9	0.994
	20	107.6	103.9	8.3	103.9	1.5	10.7	0.996
0.5	2	115.2	112.4	41.3	78.0	1.5	8.9	0.995
	5	113.6	110.3	24.1	110.0	1.3	9.4	0.995
	10	111.9	107.9	11.4	107.2	1.6	11.9	0.995
	15	110.5	106.3	9.9	104.4	1.8	11.5	0.993
	20	109.1	105.0	7.6	103.6	1.6	11.1	0.996
3	2	114.7	111.5	55.9	65.0	1.7	7.4	0.998
	5	112.8	109.1	30.4	98.2	1.2	8.4	0.998
	10	110.6	106.8	16.5	97.6	1.4	10.3	0.995
	15	109.6	105.0	11.2	96.9	1.7	11.1	0.994
	20	108.1	103.6	8.1	96.7	1.5	10.9	0.997
5	2	114.7	111.0	54.6	66.8	1.6	8.0	0.999
	5	112.9	108.4	32.0	101.4	1.1	8.6	0.999
	10	111.2	105.5	19.2	98.0	1.4	10.2	0.997
	15	109.4	103.2	13.5	95.2	1.5	10.8	0.996
	20	108.2	101.4	10.7	94.0	1.4	10.6	0.998

attributed to folding of nanosheets [17]. The image shows separated sheets with size between 2-3 microns in lateral dimension. The presence of wrinkles on graphene sheets is attributed to the residual oxy-functional groups on graphene surface [18]. On the other hand, CB particles in Figure 1D showed considerably aggregated structures even when precipitated from highly dilute solutions. The aggregated structure shows fractals with sizes ranging to several microns [9].

3.2. Morphology and dispersion in nanocomposites

The morphology of nanocomposites was studied using scanning electron microscopy (SEM) and transmission electron microscopy (TEM). Neat PE showed a smooth fractured surface (Figure 2A). The cryogenically fractured nanocomposites of PE/TRG (Figure 2B) showed graphene sheets pulled out during cryo-fracturing, showing fibrous morphology. Increasing in the TRG filler percentages to 5wt% (Figure 2C) showed a better surface as TRG works as a nucleation agent. The dispersion of graphene in PE was also studied using TEM (Figure 2D). The TEM image indicated that TRG was properly dispersed in PE with some graphene accumulation at the edges.

3.3. Thermal characterization of nanocomposites

Thermal history removed samples were cooled from 140 °C to equilibrium temperature for recording crystallization temperature (T_c) followed by subsequent heating to record melting temperatures (T_m) at 10 °C/min. The observed T_m and T_c values for neat PE were ~122 °C and ~105 °C, respectively. The neat PE exhibited smooth transitions temperatures, showing the absence of any low molecular weight impurity.

The cooling profiles of nanocomposites are shown in Figure 3 (a, b). A single crystallization exotherm was observed for all nanocomposites. Incorporating fillers altered the characteristic onset (Onset-T_c) and peak crystallization (peak-T_c) temperatures in addition to peak broadening/ stretching during crystallization. The Onset-T_c increased with increasing graphene contents, attributed to the nucleating effects. The nucleation continued until 0.5 wt% graphene loading that reduced at 3 and 5 wt% TRG. A decrease in Onset-T_c at higher TRG concentrations might be associated with the self-agglomeration of graphene sheets. No significant change was observed in the characteristic peak values of T_c and T_m with increasing graphene concentrations. This is a usual pattern observed in graphene-based nanocomposites reported before [9]. The Onset-T_c, peak-T_c, and crystallization peak end temperatures along with melting characteristics are provided in Table 1. The enthalpies were calculated by integrating area under the curves. The percentage of crystallinity was calculated as follows:

$$X_c(\%) = \frac{\Delta H_m}{\Delta H_{100\%}(1-\theta)} \times 100\% \quad (1)$$

Here, X_c % represents percentage crystallinity of PE, ΔH_m is enthalpy of melting, enthalpy of melting of perfectly crystalline PE as $\Delta H_{100\%}$ (279 J/ g [19]), and θ is the weight fraction of the filler. There was no particular trend observed in Table 1 with increasing graphene loading. However, Onset-T_c increased with increasing graphene loading. A similar trend was observed in PE/CB composites (Table 2).

Table 6. Nonisothermal crystallization parameters for PE/CB.

CB wt%	ϕ	T_o	T_p	$t_{1/2}$	ΔH_c	Avrami Fitting		
	(°C/min)	(°C)	(°C)	(s)	(J/g)	n	k_c (min) (10)	R^2
0.5	2	114.7	111.0	155.8	97.4	1.0	10.6	0.999
	5	113.1	108.7	65.3	93.3	1.0	12.3	1.000
	10	110.3	106.5	34.7	90.2	1.2	16.4	0.998
	15	109.1	104.9	24.1	88.8	1.0	21.3	1.000
	20	108.1	103.6	20.6	87.6	1.0	27.8	0.998
1.5	2	115.7	111.4	177.2	109.0	1.1	10.3	1.000
	5	113.4	108.9	84.7	100.5	1.1	12.3	1.000
	10	111.3	106.4	48.5	96.3	1.0	16.2	1.000
	15	109.7	104.6	33.9	95.2	1.0	21.2	1.000
	20	108.8	103.1	26.2	95.0	1.1	27.7	1.000
3	2	117.2	112.0	174.4	106.5	1.4	10.6	0.997
	5	114.5	109.7	85.2	101.9	1.1	12.3	1.000
	10	112.8	107.5	49.5	98.0	1.2	16.4	0.999
	15	111.2	106.0	37.8	96.4	1.3	21.3	0.999
	20	109.6	104.7	27.1	96.1	1.2	27.8	0.999
4.3	2	116.1	111.9	198.3	112.2	1.5	11.0	0.993
	5	114.7	109.8	90.1	102.4	1.2	12.7	0.999
	10	113.3	107.5	51.9	99.0	1.2	17.2	0.998
	15	111.5	106.0	37.3	96.5	1.3	21.6	0.998
	20	110.0	104.6	30.0	94.6	1.2	28.1	0.999
6.5	2	117.0	112.2	155.6	74.1	1.7	10.8	0.994
	5	115.7	110.2	82.6	93.6	1.3	12.5	0.999
	10	113.6	108.1	47.0	91.6	1.2	16.6	0.997
	15	112.5	106.6	33.4	90.3	1.3	21.4	0.998
	20	111.6	105.1	25.9	89.9	1.2	28.0	0.999
10	2	114.4	111.1	173.0	106.5	1.0	10.9	1.000
	5	112.6	108.6	80.6	100.0	1.0	12.6	0.997
	10	110.4	106.0	46.2	96.4	0.9	16.6	0.999
	15	109.2	104.1	32.2	94.0	0.9	21.7	0.999
	20	107.9	102.6	24.8	93.6	1.0	28.3	1.000

3.4. Isothermal crystallization kinetics

The isothermal crystallization was studied at four selected temperatures: 106°, 108°, 110°, and 112 °C. The samples were quenched quickly from 140 °C to avoid premature crystallization before reaching selected T_c [8, 20]. Following the complete crystallization at selected T_c, samples were cooled to equilibrium temperature and subsequently heated to 140 °C at 10 °C/min to record T_m associated with the selected T_c.

At T_c = 106 °C, small shoulder exhibited by neat PE is attributed to premature crystallization. Increasing TRG loading shifted the crystallization peak time (time to reach 100% crystallization) towards lower values, because of the nucleation effect. A significant change was observed at 0.5 wt% TRG loading where the peak time moved from 33s for neat PE to 26.5s for 0.5% PE/TRG nanocomposites. Increasing graphene concentration exhibited adverse effects on crystallization with peak broadening at 3% graphene and a very broad peak at a graphene loading of 5 wt%. A similar trend was observed in PE/CB composites. The crystallization peak time decreased from 27.4s to 23.5s as CB loading changed from 3 wt% to 6.5 wt%. A completely distorted peak was observed at 10 wt% CB.

Isothermal crystallization data was converted into fractional (relative) crystallinity as a function of t-t_o time where t_o is the crystallization onset time (Figure 3 (e, f)). The Avrami equation was used to analyze both isothermal and nonisothermal crystallization kinetics [21]. The Avrami equation is expressed as follows [22]:

$$X(t) = 1 - \exp(-kt^n) \tag{2}$$

here, $X(t)$ is the fraction crystallized at time t, n the Avrami index (representing the dimensionality of the growing crystals, and predicts an instantaneous or sporadic nucleation), k is the overall crystallization rate constant (containing the contributions from both nucleation and growth), and t is crystallization time in seconds [22, 23]. A nonlinear fitting of the Avrami equation to the experimental data yielded various Avrami parameters for PE/TRG nanocomposites (Table 3) and PE/CB composites data in Table 4. With increasing crystallization temperature, the nanocomposites took a longer time to crystallize.

The crystallization half time ($t_{1/2}$) defined as the time required by a material to achieve 50% crystallization, is considered pertinent in understanding crystallization kinetics. In general, lower $t_{1/2}$ indicates faster crystallization. In both types of composites, experimental $t_{1/2}$ increased with increasing crystallization temperature, which is attributed to energetic chains becoming difficult to solidify. On the other hand, $t_{1/2}$ decreased with increasing filler concentration at a specific T_c. The decrease in $t_{1/2}$ is attributed to the restricted movement of PE chains in PE/TRG nanocomposites at higher loadings. In addition, $t_{1/2}$ was also calculated using the Avrami constant, k with Eq. (3). An excellent agreement was observed between experimental and calculated $t_{1/2}$ values. The Avrami parameters from isothermal crystallization of PE/TRG nanocomposites are listed in Table 2.

$$t_{1/2} = (\ln 2 / k)^{1/n} \tag{3}$$

The energetic parameters for isothermal crystallization were evaluated by the temperature dependent Lauritzen-Hoffman (LH) theory [24]. The LH theory represents linear growth of crystals in polymers.
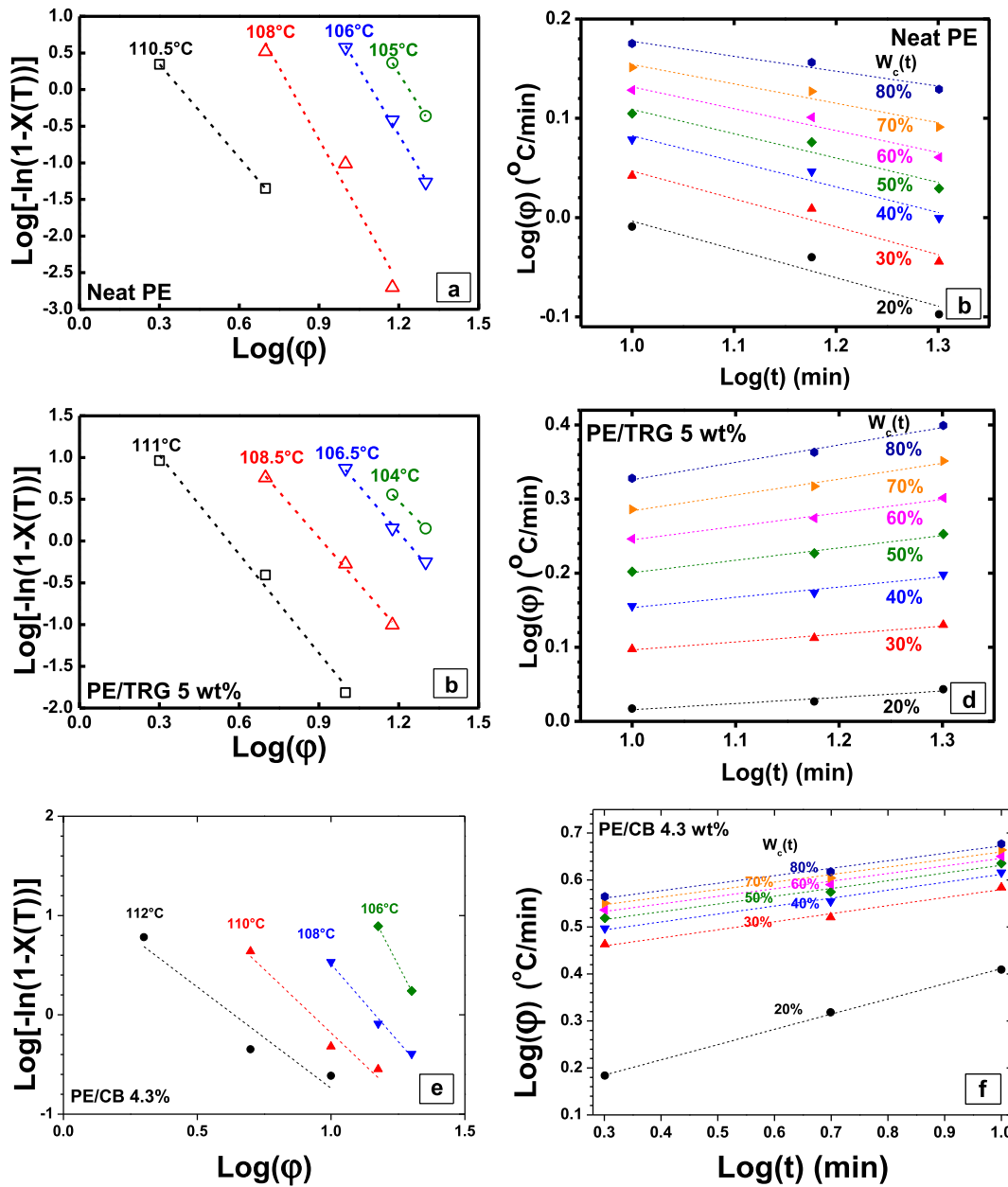
Figure 5. Representative Ozawa plots (a, c, e), Mo's plots (b, d, f) for neat PE, PE/TRG 5 wt% and 4.3% PE/CB nanocomposites.

According to the LH theory, growth rate of crystals during isothermal crystallization G is expressed as follows:

$$G = G_0 \exp\left(-\frac{\Delta E}{R(T_c - T_\infty)}\right)\exp\left(-\frac{K_g}{T_c \Delta T f}\right) \tag{4}$$

here, G_0 is a pre-exponential factor, R is the universal gas constant, ΔE is the activation energy of PE chains to the crystalline site (6276 J/mol), T_∞ is the temperature where all the motions associated with the viscous flow stop ($T_\infty = T_g - 30K = 113K$), and T_g is the glass transition temperature for PE = 143 K [25]. The ΔT is the supercooling temperature, defined as $\Delta T = T_m^\circ - T_c$; T_m° is the equilibrium melting temperate for PE = 395 K [25], and f is the correction factor accounting for variation of the equilibrium melting enthalpy as $f = 2T_c/(T_m^O + T_c)$. The term $[-\Delta E/R(T_c - T_\infty)]$ is used as a segmental jump rate in polymers to represent temperature dependence [26]. The factor G, representing a linear growth rate of crystals as a function of time, is defined as the inverse of the experimental $t_{1/2}$. A linear form of the LH equation is written as follows:

$$\ln G + \frac{\Delta E}{R(T_c - T_\infty)} = \ln G_0 - \frac{K_g}{T_c \Delta T f} \tag{5}$$

The nucleation constant K_g is calculated using the following expression:

$$K_g = \frac{nb_o \sigma \sigma_e T_m^o}{k \Delta H} \tag{6}$$

here, n value is a function of the LH theory-based crystallization regimes. Three regimes are identified by the LH thery (regime-I, regime-II, and regime-III) as a function of undercooling. The regime–I is observed when surface nuclei cause completion of crystal growth; regime-II represents diffusion-controlled crystal growth; and regime-III represents

Table 7. The Ozawa's parameters for nonisothermal crystallization of the composites.

TRG wt%	Ozawa's constants			CB wt%	Ozawa constant		
	T (°C)	m	K (T)		T (°C)	m	K (T)
0	110.5	2.3	1.6	0.5	111	1.2	1.8
	108	4.6	5.2		109	1.5	3.0
	106	4.1	6.7		107	2.2	4.7
	105	3.8	7.2		105	1.9	5.2
0.07	110.5	2.6	2.5	1.5	112	0.7	1.3
	108.5	2.5	3.8		109	1.2	2.9
	106.5	2.9	5.4		107	1.6	4.1
	105	2.8	6.2		105	1.9	5.2
0.16	111	2.0	1.9	3	112	-	1.3
	109	3.0	4.0		110	0.3	2.2
	107	3.2	5.7		108	1.1	3.6
	105.5	2.9	6.3		106	3.5	7.4
0.5	112	2.0	2.1	4.3	112	-	1.0
	110.5	3.1	4.3		110	0.1	2.0
	108.5	2.5	5.1		108	1.1	3.6
	107	2.0	5.2		106	3.2	7.0
3	112	2.9	1.6	6.5	113	-	0.6
	109.5	3.4	4.3		110	-	1.1
	107.5	3.3	5.7		109	-	2.2
	106	3.8	6.0		107	1.1	4.3
5	111	2.0	2.2	10	112	0.1	0.7
	108.5	1.7	3.3		110	0.7	1.8
	105.5	1.7	4.6		108	1.5	3.4
	104	1.3	4.4		106	2.1	4.8

interfacially controlled crystal growth (similar to regime I). Thus, regimes I and III are represented by n = 4 whereas regime II has n = 2.

The fold surface free energy σ_e is used to understand secondary nucleation in polymers and σ is the lateral surface energy (0.0112 J/m^2 for neat PE); b_o is thickness of surface monolayer (4.55 Å for PE), k is the Boltzmann's constant, and ΔH is the theoretical heat of fusion (ΔH for PE = 2.8 × 10^8 J/m^3) [27]. The equilibrium melting temperature T_m^o was estimated using the Hoffman-Week's theory [28]. There was a slight change in T_m^o observed in neat PE with the addition of TRG and CB.

For PE/TRG nanocomposites, K_g and σ_e showed a similar trend with increasing graphene concentration (Table 3). For neat PE, K_g was12640 K^2 and σ_e was 6.03 kJ/m^2.K. Increasing TRG concentration decreased K_g to 3076 at 5 wt% whereas σ_e decreased to a value of 1.47 at the same loading. A decreased σ_e is attributed to reduced work required to produce a new surface during the solidification process; further confirming TRG as a nucleating agent for PE [29]. Similarly, these values dropped significantly when the concentration of CB was increased beyond 3 wt% in PE/CB composites (Table 4).

3.5. Nonisothermal crystallization kinetics

Most of polymer processing and product-forming methods undergo nonisothermal conditions, leading to the significance of understanding dynamic crystallization. The molten, history-removed samples were cooled at various cooling rates φ (2, 5, 10, 15, and 20 °C/min), and crystallization exotherms were recorded. Figure 4 shows nonisothermal crystallization of selected composites at a fixed cooling rate (10 °C/min). The typical crystallization parameters such as onset of crystallization (T_o), exothermic peak maxima (T_p), and crystallization half time ($t_{1/2}$) were obtained from these thermograms (Table 5). Increasing filler concentration increased T_o, T_p, and decreased $t_{1/2}$ for both types of the composites, attributed to heterogeneous nucleating effects of fillers [7,

8]. Increasing graphene concentration from 0 (neat PE) to 0.5 wt% increased T_p from 105.7 °C to 107.9 °C, respectively, which decreased to 105.5 °C at 5 wt% loading. The increase in T_p with TRG indicates expectedly increased nucleation and formation of a thicker interface [7]. On the other hand, a peak value of T_p = 108.1 °C was observed at 0.5 wt % CB reduced to 106 °C for 10 wt% CB concentration (Table 6). Furthermore, increasing cooling rate (φ) decreased T_p for composites, which is attributed to lower temperature nucleation of the crystallites at higher φ values [7]. Higher the φ, restricted are the molecules; leading to decreased nucleation because the system reaches a lower temperature before nuclei could emerge [7, 29]. The enthalpy of crystallization (ΔH_c) (calculated from the area under the crystallization curve), a direct indication of percentage crystallinity, also decreased with increasing the filler concentration as well as increasing φ (see Tables 5 and 6).

In order to evaluation crystallization kinetics, temperature-scale experimental crystallization data should be converted into a time scale. The nonisothermal crystallization data (function of temperature) was converted time scale using following equation [30]:

$$t = \frac{T_o - T}{\phi} \tag{7}$$

Figure 4 (c, d) show fractional crystallinity of neat PE as a function of temperature and time. The $t_{1/2}$ decreased with increasing φ. Furthermore, the apparent $t_{1/2}$ for neat PE decreased with increasing graphene concentration. The $t_{1/2}$ decreased with instant TRG addition (Table 5), confirming the nucleating characteristics of graphene. On the other hand, there were not significant changes in $t_{1/2}$ for PE/CB composites as expected (Table 6).

3.5.1. Analysis of nonisothermal crystallization kinetics

The fractional crystallinity evolved during nonisothermal crystallization was also studied using the Avrami, Ozawa, and Mo's kinetic models. These models are frequently used to understand structural

development during the course of crystallization under dynamic conditions. The following sections contain an analysis of nonisothermal crystallization data using the above mentioned theories.

3.5.2. Avrami analysis

The Avrami equation is traditionally developed for isothermal crystallization. In order to evaluate nonisothermal kinetics, temperature-scaled fractional crystallinity was converted into a time-scaled crystallinity [30]. Using the time variation, experimental data could be treated by the methods used for isothermal kinetic analysis. However, Jeziorny [31] proposed a correction factor called corrected crystallization rate for nonisothermal crystallization (k_c) to replace the Avrami crystallization rate (Eq. 8) The Jeziory's correction follows that crystallization rate should be adjusted to accommodate constant ϕ-experiment [31]. The time-dependent crystallization data exhibited an excellent fit with the Avrami equation (Figure 4d, Table 5).

$$\log k_c = \frac{\log k}{|\phi|} \tag{8}$$

The Avrami parameters of nanocomposites exhibited patterns similar to what was shown by Liu [32]. The Avrami exponent, n is related to the type of nucleation and growth geometry of the crystals. Although the Avrami exponent does not define a unique nucleation and growth process; there is a possibility that a relationship can be made between n, crystallization mechanisms, and the morphology and structure in the crystalline state [33]. On average, an exponent of 1.6 for neat PE crystallized at all temperatures is consistent with the two-dimensional spherical crystal growth process. With the addition of 0.07 wt% TRG, n value reduced to 1.4, 1.6 at 0.5 wt% TRG, and reduced to 1.4 at 5 wt% TRG. Although the assumptions used to derive the Avrami equation should result in n being integer values for the homogenous nucleation and linear growth processes, the non-integer value could be expected in heterogeneous nucleation processes due to mixed nucleation modes [34].

Table 8. Mo's theory parameters for nanocomposites.

TRG wt%	W_c (t)%	F(T)	a	R^2	CB wt%	W_c (t)%	F(T)	a	R^2
0	20	1.9	0.3	0.857	0.5	20	2.0	-0.1	0.955
	30	2.1	0.3	0.895		30	2.2	-0.1	0.956
	40	2.2	0.3	0.919		40	2.4	-0.1	0.956
	50	2.3	0.2	0.894		50	2.5	-0.1	0.955
	60	2.2	0.2	0.917		60	2.6	-0.1	0.947
	70	2.2	0.2	0.912		70	2.7	-0.1	0.950
	80	2.1	0.2	0.924		80	2.8	-0.1	0.941
0.07	20	1.5	0.1	0.890	1.5	20	2.0	-0.2	1.000
	30	1.6	0.1	0.848		30	2.3	-0.2	1.000
	40	1.7	0.1	0.896		40	2.4	-0.2	1.000
	50	1.8	0.0	0.582		50	2.6	-0.2	1.000
	60	1.9	0.0	0.644		60	2.7	-0.2	1.000
	70	2.0	0.0	0.852		70	2.8	-0.2	1.000
	80	2.0	0.0	0.786		80	2.9	-0.2	1.000
0.16	20	1.3	0.1	0.878	3	20	1.6	-0.3	1.000
	30	1.5	0.1	0.943		30	2.1	-0.2	1.000
	40	1.6	0.1	0.833		40	2.3	-0.2	1.000
	50	1.7	0.1	0.916		50	2.5	-0.2	1.000
	60	1.7	0.0	0.849		60	2.6	-0.2	1.000
	70	1.7	0.0	0.945		70	2.8	-0.2	1.000
	80	1.8	0.0	0.360		80	2.9	-0.2	1.000
0.5	20	0.2	-0.5	0.665	4.3	20	1.2	-0.3	0.998
	30	0.2	-0.5	0.695		30	2.6	-0.2	0.977
	40	0.3	-0.5	0.732		40	2.8	-0.2	0.981
	50	0.4	-0.4	0.716		50	2.9	-0.2	0.977
	60	0.4	-0.4	0.747		60	3.1	-0.2	0.975
	70	0.5	-0.4	0.803		70	3.2	-0.2	0.975
	80	0.5	-0.4	0.809		80	3.3	-0.2	0.974
3	20	1.1	0.1	-0.023	6.5	20	0.5	-0.5	0.963
	30	1.3	0.0	-0.081		30	0.7	-0.4	0.980
	40	1.4	0.0	-0.341		40	1.2	-0.4	0.977
	50	1.4	0.0	-0.488		50	2.2	-0.3	0.965
	60	1.5	0.0	-0.967		60	2.4	-0.3	0.962
	70	1.5	0.0	-0.144		70	2.6	-0.2	0.965
	80	1.5	0.0	0.511		80	2.8	-0.2	0.967
5	20	0.9	-0.1	0.877	10	20	2.1	-0.2	0.996
	30	1.0	-0.1	0.959		30	2.3	-0.2	0.997
	40	1.0	-0.1	0.932		40	2.4	-0.2	0.996
	50	1.1	-0.2	0.974		50	2.5	-0.2	0.996
	60	1.2	-0.2	0.985		60	2.7	-0.2	0.995
	70	1.2	-0.2	0.969		70	2.8	-0.2	0.995
	80	1.2	-0.2	0.978		80	2.9	-0.2	0.995

In general, along with excellent Avrami fit, n value in the range of 1–2 indicated two-dimensional growth PE/TRG nanocomposites. The PE/CB composites showed similar behavior with n hitting the lower end of the same range (closer to a value of 1) (Table 6).

3.5.3. Ozawa's analysis

Ozawa's crystallization theory assumes that crystallization occurs at a constant rate, and crystals grow from an initial distribution of the nuclei in the form of spherulites (3D crystals with a constant growth radius at a given temperature) [35]. The Ozawa's theory further assumes that crystallization process is essentially a result of small isothermal crystallization steps. The temperature-dependent relative crystallinity, X(T), is a function of ϕ, shown as [36]:

$$1 - X(T) = \exp(-k(T) / \phi^n) \qquad (9)$$

Here, $k(T)$ is the crystallization rate constant as a function of temperature, and n = m + 2 where m is Ozawa's parameter, which is a function of the dimensions of crystal growth and nucleation mechanism. The linearized Ozawa's equation is represented as follows:

$$\log[-\ln(1 - X(T))] = \log K(T) - n \log \phi \qquad (10)$$

Fitting the experimental data into linearized Ozawa's equation was attempted and values of k (T) and m were estimated from slope and intercept of straight lines, respectively (Figure 5 (a, b)). The averaged values of Ozawa's constant were 3.7, 2.7, 2.8, 2.4, 3.4, and 1.7 for neat PE, 0.07 wt%, 0.16 wt%, 0.5 wt%, 3 wt%, and 5 wt% PE/TRG nanocomposites, respectively. Higher values of m were expected compared to averaged values of the Avrami exponent [21]. Similarly, averaged m decreased from 1.7 at 0.5 wt% CB to 1.1 at 10 wt% CB in PE/CB composites (Table 7). An m value of 2–3 corresponds to instantaneous nucleation and growth of spheres in 3D [21]. The PE/TRG nanocomposites showed excellent agreement with Ozawa's theory whereas the PE/CB composites did not show very good fittings (Table 7). A few previous reports [37, 38] also indicated unsuccessful fitting of Ozawa equation in PE-based composites. One of the possible reasons for crystallization not following Ozawa's approach might be the strong presence of secondary crystallization mechanism, which is also evident from the Avrami analysis.

3.5.4. Mo's analysis

A crystallization equation developed by Mo and coworkers [39] combines Ozawa and Avrami equations to describe nonisothermal crystallization kinetics. The applicability of the MO equation has been reported in the crystallization of various kinds of nanocomposite systems [32, 36, 38]. It represents a relationship between the cooling rate, ϕ and time, t, at fixed levels of crystallinity as follows:

$$\phi = \frac{[k(T)/k]^{\frac{1}{m}}}{t^a} = \frac{F(T)}{t^a} = F(T)t^{-a} \qquad (11)$$

$$\log \phi = \log F(T) - a \log t \qquad (12)$$

here, a is the ratio of the Avrami's exponent "n" to the Ozawa's exponent "m" (i.e. $a = n/m$), the term $[k(T)/k]^{1/m}$ represents the value of cooling/heating rate at a certain degree of crystallinity (for simplicity, it is equal to F(T)).

The exponent "a" and F (T) were estimated at fixed % crystallinity (Figure 5 c, d). The crystallization data did not fit with Mo's model. However, the trend of F (T) as a function of W_c% was the same as reported earlier for polyamide/graphene oxide nanocomposites [40]. The value of F (T) increased with increasing W_c (Table 8), indicating a lower crystallization rate required to reach a certain degree of crystallinity at a set time. On the other hand, the exponent "a" which is the ratio of the Avrami to Ozawa's constants did not yield a proper value. Similar behavior was observed for PE/CB composites (Table 8).

4. Conclusion

Graphite oxide was thermally exfoliated and reduced into thermally reduced graphene (TRG) and confirmed using XRD, Raman spectroscopy, and TEM. The composites prepared using TRG and CB with varying filler concentrations were crystallized from melt under isothermal and dynamic conditions. A complete parametrization of crystallization kinetics was reported. The results reveal that both TRG and CB acted as nucleating agents promoting crystallization under isothermal conditions. The isothermal data showed an excellent fit with Avrami model with n value ranging 2–3 (non-integer values), attributed to heterogeneous crystallization of PE chains on TRG surface. The $t_{1/2}$ decreased with increasing TRG concentration, further confirming graphene as a nucleating agent. The Lauritzen-Hoffman treatment of the crystallization data showed a reduction in energy required to crystallize with increasing filler concentrations (for both TRG and CB). The surface energy dropped from 6.03 for neat PE to 1.47 for 5 wt% TRG and to a value of -4.43 kJ/m^2 at 10 wt% CB. During nonisothermal crystallization, T_p increased with increasing TRG concentration up to percolation followed by a decrease with further increasing TRG concentration. The enthalpy of crystallization decreased with increasing ϕ at all concentrations. The $t_{1/2}$ decreased with increasing ϕ indicating faster crystallization. Furthermore, dynamic data exhibited excellent fit with modified Avrami and Ozawa models whereas the MO's model did not provide a good fit for both types of composites. With increasing filler concentration, crystals grew from as one-dimensional rods with an instantaneous growth as predicted by the Avrami theory.

Declarations

References

[1] L.S. Schadler, L.C. Brinson, W.G. Sawyer, Polymer nanocomposites: a small part of the story, JOM 59 (3) (2007) 53–60.

[2] Y. Fukuyama, et al., The effect of the addition of polypropylene grafted SiO 2 nanoparticle on the crystallization behavior of isotactic polypropylene, J. Therm. Anal. Calorim. 113 (3) (2013) 1511–1519.

[3] R.K. Prud'Homme, et al., Thermally exfoliated graphite oxide, The Trustees of Princeton University, Princeton, NJ, US, 2010.

[4] M.Z. Iqbal, A.A. Abdala, Oil spill cleanup using graphene, Environ. Sci. Pollut. Res. Int. 20 (5) (2013) 3271–3279.

[5] C. Bao, et al., Functionalized graphene oxide for fire safety applications of polymers: a combination of condensed phase flame retardant strategies, J. Mater. Chem. 22 (43) (2012) 23057–23063.

[6] S. Cheng, et al., Reduced graphene oxide-induced polyethylene crystallization in solution and nanocomposites, Macromolecules 45 (2) (2011) 993–1000.

[7] Y. Fan, et al., Effect of clay dispersion on the nonisothermal and isothermal crystallization behaviors of polyethylene composites, Polym. Plast. Technol. Eng. 56 (15) (2017) 1646–1656.

[8] E. Tarani, et al., Insights into crystallization and melting of high density polyethylene/graphene nanocomposites studied by fast scanning calorimetry, Polym. Test. 67 (2018) 349–358.

[9] M.Z. Iqbal, et al., Processable conductive graphene/polyethylene nanocomposites: effects of graphene dispersion and polyethylene blending with oxidized polyethylene on rheology and microstructure, Polymer 98 (2016) 143–155.

[10] Z. Jin, et al., Mechanically assisted exfoliation and functionalization of thermally converted graphene sheets, Chem. Mater. 21 (14) (2009) 3045–3047.

[11] D.C. Marcano, et al., Improved synthesis of graphene oxide, ACS Nano 4 (8) (2010) 4806–4814.

[12] B.D. Cullity, Elements of X-ray Diffraction, in: Addison-Wesley Series in Metallurgy and Materials, 2 ed., Addison-Wesley Pub. Co, Reading, Mass, 1978.

[13] B.Y. Chang, et al., Facile hydrothermal preparation of titanium dioxide decorated reduced graphene oxide nanocomposite, Int. J. Nanomed. 7 (2012) 3379–3387.

[14] A.C. Ferrari, D.M. Basko, Raman spectroscopy as a versatile tool for studying the properties of graphene, Nat. Nanotechnol. 8 (4) (2013) 235–246.

[15] A.C. Ferrari, Raman spectroscopy of graphene and graphite: disorder, electron–phonon coupling, doping and nonadiabatic effects, Solid State Commun. 143 (1-2) (2007) 47–57.

[16] A.C. Ferrari, J. Robertson, Resonant Raman spectroscopy of disordered, amorphous, and diamondlike carbon, Phys. Rev. B 64 (7) (2001), 075414.

[17] M.Z. Iqbal, A.A. Abdala, Oil spill cleanup using graphene, Environ. Sci. Pollut. Control Ser. 20 (5) (2013) 3271–3279.

[18] M.Z. Iqbal, Structure-property relationships in graphene/polymer nanocomposites, in: Chemical Engineering, Colorado School of Mines. Arthur Lakes Library: Colorado School of Mines. Arthur Lakes Library, 2016, p. 196.

[19] X. Wang, et al., Dielectric properties and crystalline morphology of low density polyethylene blended with metallocene catalyzed polyethylene, IEEE Trans. Dielectr. Electr. Insul. 15 (2) (2008) 319–326.

[20] L. Li, et al., Carbon nanotube induced polymer crystallization: the formation of nanohybrid shish-kebabs, Polymer 50 (4) (2009) 953–965.

[21] E. Piorkowska, A. Galeski, J.-M. Haudin, Critical assessment of overall crystallization kinetics theories and predictions, Prog. Polym. Sci. 31 (6) (2006) 549–575.

[22] A.T. Lorenzo, et al., DSC isothermal polymer crystallization kinetics measurements and the use of the Avrami equation to fit the data: guidelines to avoid common problems, Polym. Test. 26 (2) (2007) 222–231.

[23] L.H. Sperling, Introduction to Physical Polymer Science, fourth ed., Wiley, Hoboken, N.J, 2006.

[24] F.S. Bates, G.H. Fredrickson, Block copolymers-designer soft materials, Phys. Today 52 (2000).

[25] M. Pracella, et al., Polycarbonate-linear low density polyethylene blends: thermal and dynamic-mechanical properties, J. Mater. Sci. 25 (8) (1990) 3693–3700.

[26] Z. Guang, L. Chuncheng, L. Zhenyi, The effects of alkali dehydroabietate on the crystallization process of polypropylene, Eur. Polym. J. 37 (37) (2001) 1007–1013.

[27] J.D. Hoffman, Regime III crystallization in melt-crystallized polymers: the variable cluster model of chain folding, Polymer 24 (1) (1983) 3–26.

[28] M.Z. Iqbal, A.A. Abdala, M.W. Liberatore, Synthesis and characterization of polyethylene/oxidized polyethylene miscible blends and role of OPE as a viscosity control, J. Appl. Polym. Sci. 133 (28) (2016) 43521–43532.

[29] Y. Gao, et al., Functionalized multi-walled carbon nanotubes improve nonisothermal crystallization of poly(ethylene terephthalate), Polym. Test. 27 (2) (2008) 179–188.

[30] C.C.N. de Melo, et al., Analysis of nonisothermal crystallization kinetics of graphene oxide - reinforced polyamide 6 nanocomposites, Thermochim. Acta 667 (2018) 111–121.

[31] A. Jeziorny, Parameters characterizing the kinetics of the non-isothermal crystallization of poly (ethylene terephthalate) determined by DSC, Polymer 10 (10) (1978) 1142–1144.

[32] S. Liu, et al., Isothermal and nonisothermal crystallization kinetics of nylon-11, J. Appl. Polym. Sci. 70 (12) (1998) 2371–2380.

[33] L. Mandelkern, Crystallization of Polymers: Volume 2, Kinetics and Mechanisms, Cambridge University Press, 2004.

[34] C. Ferreira, et al., Isothermal and non-isothermal crystallization kinetics of polypropylene/exfoliated graphite nanocomposites, Thermochim. Acta 553 (2013) 40–48.

[35] T. Ozawa, Kinetics of non-isothermal crystallization, Polymer 12 (3) (1971) 150–158.

[36] T. Liu, Z. Mo, H. Zhang, Nonisothermal crystallization behavior of a novel poly(aryl ether ketone): PEDEKmK, J. Appl. Polym. Sci. 67 (5) (1998) 815–821.

[37] T.G. Gopakumar, et al., Influence of clay exfoliation on the physical properties of montmorillonite/polyethylene composites, Polymer 43 (20) (2002) 5483–5491.

[38] S.P. Lonkar, et al., Preparation and nonisothermal crystallization behavior of polypropylene/layered double hydroxide nanocomposites, Polymer 50 (6) (2009) 1505–1515.

[39] M. Liu, et al., Melting behaviors, isothermal and non-isothermal crystallization kinetics of nylon 1212, Polymer 44 (8) (2003) 2537–2545.

[40] C.C.N. de Melo, et al., Analysis of nonisothermal crystallization kinetics of graphene oxide-reinforced polyamide 6 nanocomposites, Thermochim. Acta 667 (2018) 111–121.